JASA EXPRESS LETTERS ARTICLE asa.scitation.org/journal/jel

Effect of ocean eddies on seismic *T* waves

Shane Zhang,[1,a] Shirui Peng,[1,b] Haakon L. L. Ervik,[1,c] Zhichao Shen,[2,d] Wenbo Wu,[2,e] Zhongwen Zhan,[1,f] and Jörn Callies[1,g]
[1]*Division of Geological and Planetary Sciences, California Institute of Technology, Pasadena, California 91125, USA*
[2]*Department of Geology and Geophysics, Woods Hole Oceanographic Institution, Woods Hole, Massachusetts 02543, USA*

Note: This article is part of a Special Issue on Climate Change: How the Sound of the Planet Reflects the Health of the Planet.

Abstract: Earthquakes excite sound waves along continental margins, *T* waves, that can propagate for thousands of kilometers in the ocean. The complex *T* waveforms are shaped by the extended region of seismic-to-acoustic conversion. Because the conversion has a width comparable to ocean eddies, *T* waveforms can be modified substantially by the subsequent propagation through eddies. Sound speed anomalies associated with eddies shift arrival times, so waves arriving from different azimuths can have experienced different phase shifts, making the recorded waveform an eddy-dependent interference pattern. Leveraging this multipath propagation can improve the spatial resolution of deep-ocean temperature change estimated with *T* waves.

[Editor: Ying-Tsong Lin] https://doi.org/10.1121/10.0041805

Received: 6 August 2025 **Accepted:** 20 November 2025 **Published Online:** 8 December 2025

1. Introduction

About 90% of the excess energy from anthropogenic climate forcing is absorbed by the ocean (Intergovernmental Panel on Climate Change, 2021), causing warming and contributing to sea level rise. To sharpen predictions of the future climate, we need to better constrain where and how fast heat is transported from the surface to the deep ocean. Observing current and past ocean temperature changes is key to understanding this heat transport and to improving its representation in climate models.

The interior ocean's temperature can be taken *in situ* with instruments lowered from ships (e.g., Talley *et al.*, 2016) or attached to autonomous platforms (e.g., Wong *et al.*, 2020), or it can be constrained remotely using acoustics (Munk and Wunsch, 1979; Munk *et al.*, 1995). *In situ* data is sparse and aliases temperature fluctuations because of mesoscale eddies and other small-scale transients. Acoustic measurements, as originally demonstrated using active-source acoustics (e.g., The ATOC Consortium, 1998; Dushaw *et al.*, 2009; Gemba *et al.*, 2023), take advantage of the temperature dependence of the sound speed and provide path-integrated measurements that naturally average over small-scale transients. The adoption of such active-source acoustic tomography has been slow, however, and passive approaches have been developed in response, using ambient sound (Woolfe *et al.*, 2015; Evers *et al.*, 2017; Tan and Godin, 2021; Ragland *et al.*, 2024) or submarine volcanoes (Smets *et al.*, 2022) as natural sources. Recently, a new passive acoustic approach has been developed (Wu *et al.*, 2020; Callies *et al.*, 2023; Wu *et al.*, 2023; Peng *et al.*, 2024) that uses acoustic waves excited by repeating earthquakes, so-called *T* waves (Okal, 2008).

This *T* wave approach to ocean acoustic tomography first identifies repeating earthquakes (repeaters) at land stations, which occur at different times but generate nearly identical seismic waveforms [Fig. 1(c); Wu *et al.*, 2020; Peng *et al.*, 2024]. Then changes in the low-frequency (2–3 Hz) *T* wave travel times, which are dominated by temperature change along the propagation path to a receiving hydrophone or island station, are measured by maximizing the cross correlation of the repeaters' waveforms. The approach has been demonstrated successfully for *T* waves generated at the Sunda Trench and received at Diego Garcia (Wu *et al.*, 2020) as well as Cape Leeuwin (Wu *et al.*, 2023; Callies *et al.*, 2023) and for *T* waves generated at the Japan Trench and received at Wake Island (Peng *et al.*, 2024), where temperature changes inferred from *T* waves are consistent with and complement existing sparse *in situ* observations (Peng and Callies, 2025).

[a]Corresponding author: sdz@caltech.edu
[b]Current address: Department of Earth, Atmospheric, and Planetary Sciences, Massachusetts Institute of Technology, Cambridge, MA 02139, USA. Email: speng3@mit.edu
[c]Email: haakon@caltech.edu
[d]Email: zhichao.shen@whoi.edu
[e]Current address: Department of Earth and Planetary Science, University of California at Berkeley, Berkeley, CA 94720, USA. Email: wenbo.wu@berkeley.edu
[f]Email: zwzhan@caltech.edu
[g]Email: jcallies@caltech.edu

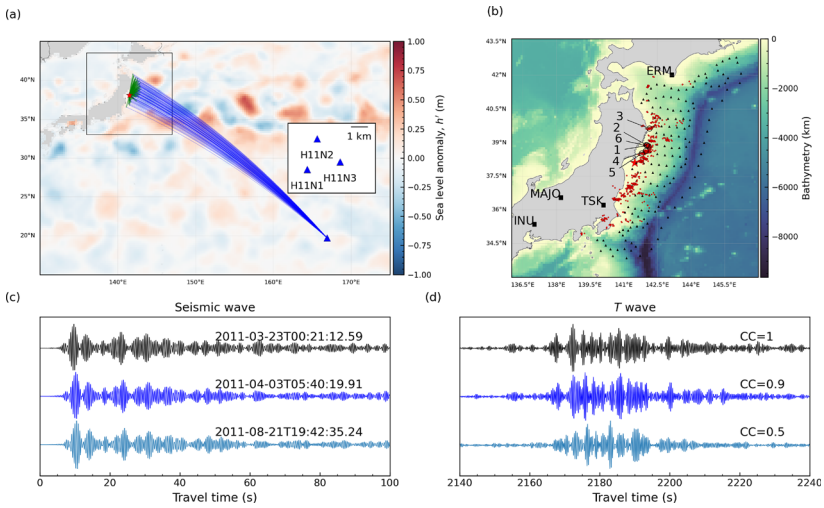

Fig. 1. The decoherence problem. (a) *T* waves propagate from an earthquake off Japan (red star) through the solid earth (green lines) and then as acoustic waves through the ocean (blue lines) to arrive at a hydrophone triad H11N (blue triangle and inset). (b) Zoom-in of the black box in (a) showing earthquake epicenters (red circles), many of which are aftershocks of the 2011 M9 Tōhoku earthquake (red star). Four land seismometers (black squares) are used to identify repeating earthquakes (Peng *et al.*, 2024), where the top six biggest repeater families are numbered. S-net ocean bottom seismometers are plotted as black triangles. (c) Seismic waveforms from three repeating earthquakes on land seismic station MAJO with origin times from the International Seismological Centre Bulletin. (d) *T* waveforms on hydrophone H11N3 from the same events.

In both of these regions, however, a significant fraction of the *T* waves from repeating earthquakes have incoherent waveforms, which precludes a reliable measurement of travel time change. Consider, for example, three repeating earthquakes on the Japan Trench with very similar seismic waveforms at the land station MAJO [Fig. 1(c)]. Only two of them also have similar *T* waveforms at the Wake Island receiver, whereas the third is distinct [Fig. 1(d)]. We quantify the waveform similarity with correlation coefficients. We call a pair of earthquakes a repeater if their seismic waveforms have a correlation coefficient above 0.9, and their cataloged properties are similar (locations and magnitudes within 50 km and 1.5, respectively) (Wu *et al.*, 2020; Peng *et al.*, 2024). A group of repeating pairs with shared events make up a repeater family [Fig. 1(b)]. We call a pair of *T* waves coherent if their correlation coefficient is above 0.6 and incoherent otherwise. About 40% and 90% of the *T* wave pairs from repeaters are incoherent for the arrivals at Diego Garcia (Wu *et al.*, 2020; Wu *et al.*, 2023) and Wake Island (Peng *et al.*, 2024), respectively. Thus far, these numerous incoherent *T* wave pairs have been dismissed and not used for temperature constraints.

Because the decoherence problem is more severe for the propagation from the Japan Trench to Wake Island, the focus of this study is to explain the *T* wave decoherence there. Decomposing the propagation path of *T* waves to the solid earth, seismic-to-acoustic conversion, and ocean, we consider the following mechanisms as candidates for the observed decoherence:

1. Earthquake location. The repeating earthquakes are actually far from one another (Igarashi, 2020), which remains unrecognized because the repeaters are identified with land stations hundreds of kilometers away [Fig. 1(b)]. Conversion from seismic to *T* waves happens at a closer distance and is more sensitive to earthquake location change.
2. Excitation. The *T* wave excitation regions is very different even for repeating earthquakes if the excitation is governed by transient features such as ocean waves (Godin, 2021).
3. Dispersion. Surface-intensified temperature change shifts higher-frequency *T* waves more than the lower frequencies (Callies *et al.*, 2023), substantially altering the received waveform.
4. Multimode, Multiple acoustic modes of *T* waves are excited, and surface-intensified temperature change affects each mode differently (D'Spain *et al.*, 2001; Park *et al.*, 2001; de Groot-Hedlin and Orcutt, 2001). If multiple modes contribute substantially to the received waveforms, this causes decoherence.
5. Refraction. *T* waves can be refracted by transient temperature gradients because of fronts (Dushaw and Menemenlis, 2014), eddies (Munk, 1980), and internal waves (Colosi *et al.*, 1994). If the propagation path is altered substantially, this causes a change in the waveform.
6. Hydrophone location. The receiving hydrophone is attached to a subsurface mooring that is displaced by currents (Nichols and Bradley, 2017). Large displacements cause changes in the recorded waveform.
7. Multipath. *T* waves are excited along an extended region along the trench (de Groot-Hedlin and Orcutt, 1999; Graeber and Piserchia, 2004) and then propagate through a field of transient mesoscale eddies. Differential travel time changes across the multipath cause decoherence.

We argue below that mechanisms 1–6 are unlikely to explain the observed decoherence (Sec. 2), whereas mechanism 7 can (Sec. 3). In Sec. 4, we then demonstrate that the multipath effect can be harnessed to obtain measurements across azimuths from single repeating pairs, expanding the information on ocean temperatures extractable from *T* wave data.

Although this study focuses on ocean acoustic tomography, the extended understanding of T waves might also help its use for detecting submarine earthquakes and volcanoes, and estimating their source properties such as location, duration, and energy flux to measure their size and tsunamigenic potential (Fox *et al.*, 2001; Okal, 2008). It might also help further refine our understanding of T wave excitation, including those excited at mid-ocean ridges rather than continental margins (cf. Graeber and Piserchia, 2004; Tolstoy and Bohnenstiehl, 2005; Okal, 2008; Bottero *et al.*, 2020; Godin, 2021; Lecoulant *et al.*, 2021; Oliveira *et al.*, 2024; Shen *et al.*, 2024).

2. Evidence against mechanisms 1–6

We use and extend the data from Peng *et al.* (2024) (Fig. 1). They used four Japanese seismic stations on land to identify a total of 18 632 repeating pairs and to obtain their origin time corrections [Fig. 1(b)]. Then they analyzed T waves excited by those earthquakes and received near Wake Island by a Comprehensive Nuclear-Test-Ban Treaty Organization (CTBTO) International Monitoring System (IMS) hydrophone (H11N3) and a seismic station on Wake Island (IU.WAKE). We focus on the data at H11N3, which recorded a total of 1566 coherent T wave pairs. Peng *et al.* (2024) then measured the travel time shifts between these coherent repeating pairs and estimated from them a time series of temperature change from 2008 to 2022.

A first possibility for the decoherence is that the repeating earthquakes might be sufficiently far from one another to excite incoherent T waves, despite their generation of almost identical seismic waveforms on land stations (mechanism 1). different seismic stations do not observe a systematic trend in origin time corrections, and explicit modeling of the location change shows that location discrepancies can only explain ∼0.02 s of the travel time change, which is much smaller than a wave period of about 0.4 s. This is unlikely because the repeaters also generate nearly identical seismic waveforms at NIED (National Research Institute for Earth Science and Disaster Resilience) S-net stations [Fig. S1(a)], ocean bottom seismometers offshore Japan that cover the region of T wave excitation [Fig. 1(b)]. Because many of the earthquakes occur beneath S-net stations, changes in the earthquake depth would be easily detectable in travel time shifts between repeaters [Fig. S1(b)].

The S-net observations also disfavor excitation differences as a plausible explanation for the decoherence (mechanism 2), showing nearly identical waveforms at the seafloor. Furthermore, we infer the apparent excitation regions of T waves by using a progressive multi-channel correlation approach between the H11N hydrophone triad (Fig. S2; Graeber and Piserchia, 2004). For the biggest repeater families, both the back-azimuths and waveform envelopes are similar between these events [Figs. 2(a) and 2(b), Fig. S3], suggesting that differences in the T wave excitation between repeaters cannot be very large. This suggests that excitation from ocean waves is less likely (Godin, 2021) than bathymetry features (Shen *et al.*, 2024). The back-azimuths vary by up to 2° [Fig. 2(a)], corresponding to an excitation region that is about 100 km wide. Using canonical seismic and acoustic wave speeds and assuming geodesic propagation on a reference ellipsoid (Burenkov *et al.*, 1994), we infer the apparent T wave excitation regions (Graeber and Piserchia, 2004), which closely track bathymetric contours [Fig. 2(c)]. This wide excitation along the trench is consistent with previous work (de Groot-Hedlin and Orcutt, 1999, 2001) and a crucial part of our favored mechanism (mechanism 7; see Sec. 3).

Dispersive T wave propagation (mechanism 3) has been observed and leveraged to obtain depth resolution in temperature estimates (Callies *et al.*, 2023), but it is likely unimportant for the decoherence of waveforms because of the narrow frequency band used. Moreover, if dispersion were important, the waveform similarity would decrease with increasing (surface-intensified) temperature change between the events, because the differential travel time change between frequencies would increase. In contrast, the T wave correlation coefficients show no marked decrease with increasing travel time change (Fig. S4).

The lack of dependence of the waveform coherence on travel time change also disfavors the multimode effect (mechanism 4). Different modes, like different frequencies, have sensitivities to temperature change with a different vertical

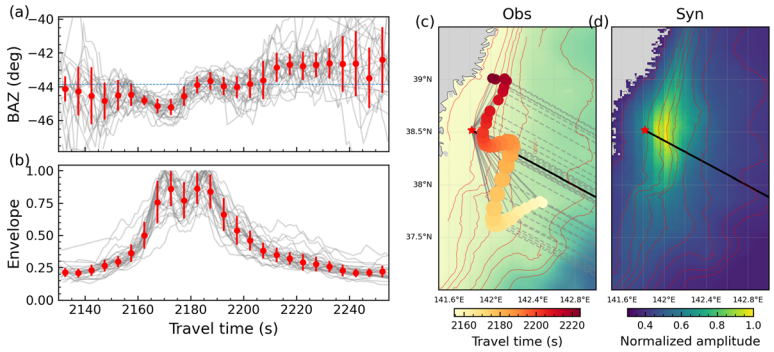

Fig. 2. Observation and modeling of T wave excitation. (a), (b) Back-azimuths and normalized envelopes for T wave from a repeater family. Each gray line is from a single event, whereas the red dots show binned average $\pm 1\sigma$. (c) Inferred excitation locations based on the family averaged back-azimuths, where the circle size is proportional to amplitude, and the travel time is color-coded. Gray lines show the paths from the epicenter to excitation locations and on to the receiver, whereas the black line denotes the geodesic between the epicenter and receiver. (d) Normalized T wave excitation amplitude from the seafloor scattering model.

structure, leading to the same expectation of greater decoherence for a larger travel time change (Fig. S6). Higher modes tend to be quickly attenuated by the seafloor at the low frequency considered here, so our T waves should be composed mainly of the fundamental mode (de Groot-Hedlin and Orcutt, 2001; Wu *et al.*, 2023).

The consistency of the back-azimuths within a repeater family [Fig. 2(a)] also disfavors the refraction effect (mechanism 5), which should cause a substantial change in apparent back-azimuth (Munk, 1980; Dushaw and Menemenlis, 2014). In addition, scattering by internal waves typically changes travel times by less than 0.01 s (Colosi *et al.*, 1994), much less than the wave period of 0.4 s.

For hydrophone displacements to substantially affect the waveform (mechanism 6), the displacements would have to be a substantial fraction of the wavelength of 600 m. Nichols and Bradley (2017) estimated displacements of CTBTO hydrophones of only a few tens of meters, which is also consistent with the attribution of Peng *et al.* (2024) of 0.03 s of travel time variability to hydrophone displacements.

In summary, mechanisms 1–6 are unlikely to explain the observed decoherence of T waveforms at the Wake Island hydrophone, leaving mechanism 7 as the only one remaining on our list. Indeed, the T wave excitation is extended and produces a multipath propagation through the ocean (Figs. 1 and 2). The multipath has a width comparable to the size of mesoscale eddies, allowing for the temperature anomalies associated with the eddies to change the interference pattern at the receiver. We quantify the impact of this effect on the waveform in the following section.

3. Multipath propagation through ocean eddies

3.1 The multipath model

We compute synthetic T waveforms by considering together the seismic wave propagation through the solid earth, conversion to acoustic waves at the seafloor, and acoustic propagation through an ocean filled with mesoscale eddies. T waves in our study region are most likely excited by scattering at the rough seafloor (de Groot-Hedlin and Orcutt, 1999, 2001) rather than downslope conversion (Johnson *et al.*, 1963; Talandier and Okal, 1998), which would be inefficient for the comparatively gentle slopes in our source region.

We closely follow de Groot-Hedlin and Orcutt (2001) in modeling the T wave propagation using adiabatic modes (supplementary material text S1, Fig. S5), except that we retain phase information incurred by mesoscale eddies. We employ a point source because most of our earthquakes have a magnitude between 3.5 and 4.5 (Peng *et al.*, 2024) and thus a much smaller rupture extent than the T wave excitation zone. We treat small-scale seafloor roughness as potential scatterers to excite T waves, such that the total pressure $\bar{p}$ felt at a hydrophone is the sum of contributions from all scatterers k,

$$\bar{p}(t) = \sum_k A_k p(t - \tau_k), \tag{1}$$

where A_k and τ_k denote the amplitude and arrival time from scatterer k, and p is a common source wavelet, which we choose to be a sinusoid with a center frequency of $f = 2.5$ Hz and a modulated envelope [Fig. S8(b)].

To model the amplitude A for each scatterer, we first account for geometrical spreading and anelastic attenuation in solid earth. Then, we use an average sound speed profile in the study region (Fig. S5) to compute the mode excitation strength as a proxy for the conversion from seismic to acoustic waves. Finally, to model transmission loss in the ocean, we consider both geometrical spreading and sea floor interaction, which is computed by integrating the mode energy leaking into the solid earth along the path from a scatterer to the receiver.

Combining all factors yields an effective excitation pattern that decays from the epicenter and is elongated along bathymetry contours [Fig. 2(d)], largely consistent with the apparent sources inferred from the hydrophone triad [Fig. 2(c)]. The modeled excitation is shifted slightly to the north compared to observations. This might partially arise from the mislocation of the hydrophone triad, which can cause back-azimuth errors up to 0.5° (Graeber and Piserchia, 2004). Another possibility is refraction by the Kuroshio front, which can bias the apparent excitation toward the South. A rough calculation using Snell's law and assuming a 1% sound speed anomaly across the front and an incidence angle of 45° gives a refraction by about 0.6°.

The arrival time τ from each scatterer has three components as follows:

$$\tau = \tau_0 + \tau' + \frac{\phi}{2\pi f}, \tag{2}$$

where τ_0 denotes a time-independent reference travel time based on canonical seismic and sound speeds, τ' denotes a time-dependent travel time perturbation arising from mesoscale eddies, and $\phi \in [0, 2\pi]$ is a time-independent and random phase shift to mimic the scattering process.

To compute the travel time perturbation τ', we use sea level anomalies as a proxy for sound speed perturbation. This is motivated by the similarity between sea level anomalies and the interior temperature anomalies sampled by T waves (Peng *et al.*, 2024). We use daily sea level data from the Copernicus Climate Change Service (2018) and remove the linear trend and seasonal cycle. The sound slowness perturbations for the fundamental acoustic mode s' that is sampled by T waves, as estimated from Argo profiles in the region, are strongly correlated to local sea level anomalies h' (Fig. S6). We use a linear regression to estimate

$$s' = ah' \quad \text{with} \quad a = -1.9 \times 10^{-6}\,\mathrm{s\,m^{-2}}. \tag{3}$$

Integrating the resulting slowness anomaly field along the ray path L from the scatterer to the receiver then gives the travel time perturbation τ',

$$\tau' = \int_L s'\, dl, \tag{4}$$

where we assume geodesic propagation on a reference ellipsoid. Having specified the amplitude and travel time for each scatterer, we sum contributions from all scatterers to compute synthetic T waves [Eq. (1), Fig. S7].

3.2 Comparing synthetics to observations

To test our excitation model, we compare the T wave durations and excitation patterns. Because the T wave excitation depends on details of the solid earth structure modeled by a random phase at excitation, we do not aim to reproduce the observed waveform wiggle-by-wiggle but only the main features. The T wave duration constrains the excitation extent (de Groot-Hedlin and Orcutt, 1999, 2001). A source-to-receiver path that is oblique to the trench axis facilitates T wave excitation across a wider region (Graeber and Piserchia, 2004). Because the path from the Japan Trench to Wake Island is nearly perpendicular to the trench, we expect a relatively confined excitation and thus a relatively short T wave duration. Synthetics indeed show a duration of only −50 s, in agreement with the observations [Fig. 3(a)]. Over the course of the arrival is also similar between the synthetics and observations [Fig. 3(b)]. The back-azimuths span about 2°, corresponding to 100 km for a source-to-receiver path of 3000 km. These numbers are comparable to the events in other studies from Kuril Island to Wake Island and from the northeast (NE) Indian Ocean to Diego Garcia but are much smaller than those from Andreanof Island to Wake Island or from NE Indian Ocean to Cape Leeuwin, where T waves propagate more parallel to the trench (de Groot-Hedlin and Orcutt, 1999; Graeber and Piserchia, 2004). In the back-azimuth evolution, both observations and synthetic show a general increase over much of the duration of the arrival [Fig. 3(b)]. Initially, the observations show a decrease, whereas the synthetics are flat. The observed decrease might be caused by the interference of waves from the two ends of the excitation zone (Fig. S7), which depends on fine-scale bathymetry and solid-earth structure. Nevertheless, the broad agreement between observations and synthetics offers support for our excitation model, which is crucial to accurately capture the impact that mesoscale eddies can have on the T waveforms.

As a further check on our synthetic T waves, we compare the travel time shifts measured from synthetics and observations [Fig. 3(c)]. The nearly one-to-one correspondence is expected, given the tight correlation between slowness and sea level anomalies (Fig. S6; Peng *et al.*, 2025).

In both the synthetics and observations, the correlation coefficients of T waves are almost always high (>0.6) for pairs of rapidly repeating earthquakes, i.e., pairs with a repeat interval of less than a month, which corresponds to the time scale of mesoscale eddies [Figs. 3(d) and 3(e)]. Because the sea level anomaly fields we use are daily, the synthetic T waves are identical for repeaters within a day, whereas the observations still show differences and, hence, lower correlation, presumably because of noise and shorter–time scale transients not captured by the sea level proxy. For repeat intervals between a few days and a month, the correlation coefficients for the synthetics decrease with the interval, as also seen in observations [Fig. 3(a)]. In contrast, in both synthetics and observations, no obvious trend between correlation and repeat interval exists for intervals longer than a month. A significant number of highly coherent repeating pairs still exists even years apart, but the majority of repeaters are weakly coherent [Fig. 3(a)].

This variability in the cross correlation is not random but shaped by mesoscale eddies; it can largely be captured by the synthetics [Fig. 3(f)]. A majority of observations have low correlations between 0.3 and 0.4, which are well represented in the synthetics. Binned averages of the correlation coefficients fall close to the one-to-one line, suggesting our model has skill in predicting the correlation between waveforms for a given pair based on the sea level anomaly field. We attribute the scatter in the correlation primarily to inaccuracies in our sea-level-based sound speed field (Fig. S6). We also assess the effect of the poorly constrained duration of the source wavelet p [Eq. (1)], which arises from uncertainties in solid-earth structure and conversion from seismic coda waves to oceanic sound waves. We find that the correlation generally increases with the source duration because at a given time window, more scatterers interfere and produce a smaller change in the waveform (Fig. S8).

In summary, the T waveform is complex but its main features such as duration [Fig. 3(a)] and excitation pattern [Fig. 3(b)] are largely reproduced by synthetics, supporting seafloor scattering as the dominant mechanism to generate T waves. Moreover, the T waveform time shifts [Fig. 3(c)], correlation time scales, and mean temporal correlations are also reproduced, suggesting that mesoscale eddies differentially changing the T wave arrival times across the multipath are the dominant effect shaping the T waveform similarity. Therefore, the multipath effect alone (mechanism 7) can largely explain the decoherence of T waves from repeating earthquakes.

4. Potential of obtaining measurements across azimuths

The extended excitation and multipath propagation of T waves can be leveraged to improve T wave ocean tomography. One can measure T wave time shifts in moving time windows and then relate each time window to a corresponding back-azimuth. We illustrate this with an example pair of repeaters [Fig. 4(a)], for which the time shift [Fig. 4(b)] clearly covaries with the back-azimuth [Fig. 4(c)], suggesting a more pronounced warming (reduction in travel time) on the southern part of the multipath. To further illustrate the azimuth-dependence, we compare time shifts between two azimuths from a

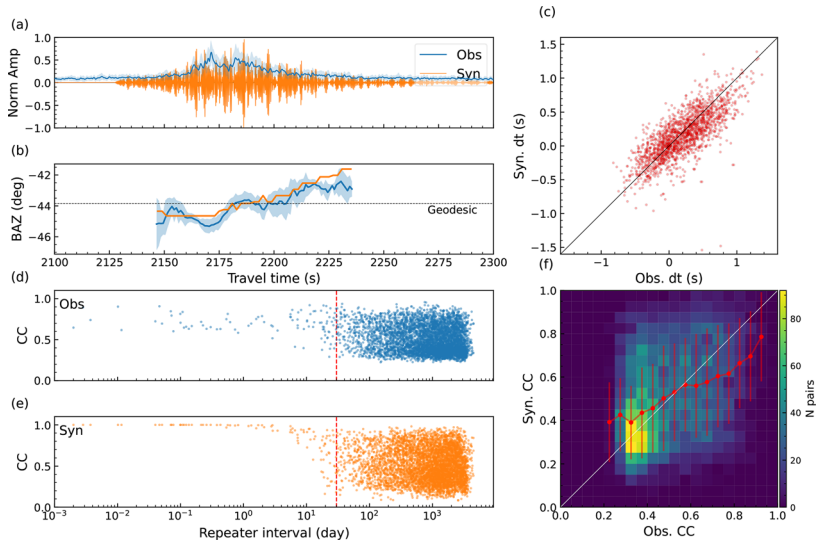

Fig. 3. Obs, observations; Syn, synthetics; CC, correlation coefficients. Synthetics explain waveform features and correlation statistics. (a), (b) Waveform envelopes and back-azimuths from synthetics ("Syn," orange) and observations ("Obs," blue) for a typical repeater family (Fig. 2). (c) Whole waveform time shift, *dt*, between repeating earthquakes from synthetics and observations. (d), (e) CCs (correlation coefficients) as a function of earthquake repeat interval for observations and synthetics. The timescale of mesoscale eddies is indicated by the red dashed line. (f) CC between repeating earthquakes from synthetics and observations. The shading shows the number of repeating pairs per bin, and the red dots are averages over observed CC bins.

family of repeaters, where we average measurements in 10 s windows centered on travel times of 2169 s and 2190 s, which correspond to back-azimuths of −44.3° and −43.7°, respectively [Fig. 4(c)]. These observed differences are correlated with the corresponding predictions based on sea level anomalies, which are converted to slowness anomalies [Eq. (3)] and then integrated along correspondent azimuths [Fig. 4(d)]. The relatively low correlation coefficient of 0.4 may be because of noise, inaccuracies in using sea level anomalies as a proxy for sound speed, and broadening of the sensitivity to a Fresnel zone surrounding the geometrical ray (e.g., Simon *et al.*, 2025). Regardless, a fan-shaped region can be constrained from a single pair of repeating earthquakes, rather than just the geodesic path from the source to the receiver. This would be particularly useful for regions with weak seismicity to provide additional azimuthal coverage and thus improve the spatiotemporal resolution of temperature estimates (cf. Peng *et al.*, 2024; Peng and Callies, 2025).

5. Conclusions

The difference in *T* waveforms produced by repeating earthquakes can be attributed primarily to the multipath propagation through a changing field of ocean eddies. For *T* waves generated by earthquakes along the Japan Trench and received at Wake Island, the excitation is wide enough such that rays received at different back-azimuths pass through different mesoscale eddies and thus experience different phase shifts between repeating earthquakes, enough to cause substantial changes to the received waveforms. This incoherence between waveforms inhibits the whole-waveform measurement of a travel time change between repeating earthquakes that has been used to constrain the deep-ocean temperature change along the *T* wave path (Wu *et al.*, 2020; Callies *et al.*, 2023; Wu *et al.*, 2023; Peng *et al.*, 2024). The improved understanding of

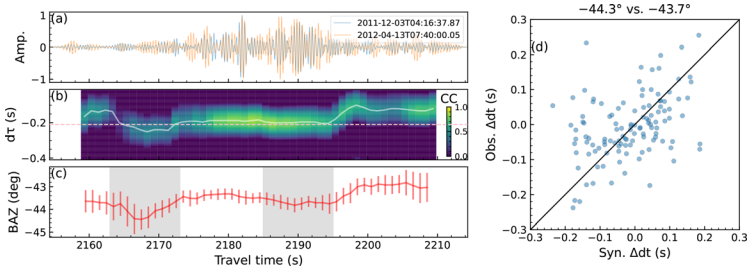

Fig. 4. Potential of obtaining measurements across azimuth. (a) *T* waveforms for an example pair of repeating earthquakes. Amplitude is normalized. (b) Moving correlation of the waveforms in (a) with a window length of 10 s. The white line shows the time shifts *dt* at the maximum CCs (correlation coefficients), whereas the pink dashed line shows the time shift, *dt*, measured from the whole waveform. (c) Back-azimuth (BAZ) variations averaged from all events in this family [Fig. 2(a)]. (d) For each event pair within this family, difference in the time shift *dt* between two back-azimuths [shadings in (c)], $\Delta dt = dt|_{\mathrm{BAZ}=-44.3^\circ} - dt|_{\mathrm{BAZ}=-43.7^\circ}$, from observations and synthetics based on sea level anomalies are plotted.

this propagation can be leveraged to make azimuth-dependent measurements over shorter time windows, which has the potential to improve the *T* wave constraints on deep-ocean temperature change and their complementarity to *in situ* measurements from Argo floats and ship-based hydrographic surveys. This may be especially useful in regions that are quieter seismically than the Sunda and Japan Trenches, which have been used for *T* wave tomography thus far.

How strong the multipath effect is depends on both the seismological and oceanographic context. How wide the excitation is depends on the shape of the seafloor and the direction of *T* wave propagation relative to the continental margin. For example, the *T* waves generated along the Sunda Trench and received at Diego Garcia propagate nearly perpendicular to the trench and through the equatorial ocean, where the deep-ocean temperature variability is dominated by planetary-scale equatorial waves rather than mesoscale eddies (Peng *et al.*, 2025), explaining the higher *T* waveform coherence observed there (Wu *et al.*, 2020; Wu *et al.*, 2023).

Confidence in the proposed model for *T* wave coherence is derived from its ability to fit the observed waveform duration, evolution of back-azimuths, and correlation coefficients between repeating earthquakes. The key assumption is that *T* waves are predominantly excited by seafloor scattering at small-scale roughness, where seafloor depths largely determine the excitation strength of *T* waves (de Groot-Hedlin and Orcutt, 1999, 2001). Future work should further evaluate the robustness of this excitation model, for example, by systematically comparing the *T* wave back-azimuth evolution estimated from observations to those produced in more complete numerical simulations of the *T* wave excitation (e.g., Bottero *et al.*, 2020; Lecoulant *et al.*, 2021).

Supplementary Material

See the supplementary material for supporting text S1 and Figs. S1–S9.

Acknowledgements

This study is supported by a SeismoLab Director's postdoc fellowship (S.Z.) and National Science Foundation Grant No. OCE-2023161.

Author Declarations

Conflict of Interest

The authors have no conflicts to disclose.

Data Availability

The IMS hydrophone data are available directly from the CTBTO upon request and signing a confidentiality agreement to access the virtual Data Exploitation Centre (vDEC). The S-net waveform data were provided by NIED (National Research Institute for Earth Science and Disaster Resilience, https://doi.org/10.17598/nied.0007). The KRAKEN software is available from Ocean Acoustics Library (OALIB) at https://oalib-acoustics.org/models-and-software/normal-modes/. The Argo data were collected and made freely available by the International Argo Program and the national programs that contribute to it (https://argo.ucsd.edu; https://www.ocean-ops.org). The Argo Program is part of the Global Ocean Observing System. The Estimating the Circulation and Climate of the Ocean (ECCO) data are available at https://doi.org/10.5067/ECG5D-OTS44 (Forget *et al.*, 2015). Bathymetry data were downloaded from and are freely available at https://download.gebco.net (GEBCO, 2023). The sea level anomaly data is available at https://doi.org/10.24381/cds.4c328c78 (Copernicus Climate Change Service, 2018).

References

Bottero, A., Cristini, P., and Komatitsch, D. (**2020**). "On the influence of slopes, source, seabed and water column properties on T waves: Generation at shore," Pure Appl. Geophys. **177**(12), 5695–5711.

Burenkov, S. V., Gavrilov, A. N., Uporin, A. Y., and Furduev, A. V. (**1994**). "Heard Island feasibility test: Long-range sound transmission from Heard Island to Krylov underwater mountain," J. Acoust. Soc. Am. **96**(4), 2458–2463.

Callies, J., Wu, W., Peng, S., and Zhan, Z. (**2023**). "Vertical-slice ocean tomography with seismic waves," Geophys. Res. Lett. **50**(8), e2023GL102881, https://doi.org/10.1029/2023GL102881.

Colosi, J. A., Flatté, S. M., and Bracher, C. (**1994**). "Internal-wave effects on 1000-km oceanic acoustic pulse propagation: Simulation and comparison with experiment," J. Acoust. Soc. Am. **96**(1), 452–468.

Copernicus Climate Change Service (**2018**). "Sea level daily gridded data from satellite observations global ocean from 1993 to present," https://cds.climate.copernicus.eu/datasets/satellite-sea-level-global?tab=overview.

de Groot-Hedlin, C. D., and Orcutt, J. A. (**1999**). "Synthesis of earthquake-generated T-waves," Geophys. Res. Lett. **26**(9), 1227–1230, https://doi.org/10.1029/1999GL900205.

de Groot-Hedlin, C. D., and Orcutt, J. A. (**2001**). "Excitation of T-phases by seafloor scattering," J. Acoust. Soc. Am. **109**(5), 1944–1954.

D'Spain, G. L., Berger, L. P., Kuperman, W. A., Kuperman, J. L., and Baker, G. E. (**2001**). "Normal mode composition of earthquake T phases," in *Monitoring the Comprehensive Nuclear-Test-Ban Treaty: Hydroacoustics*, edited by C. deGroot-Hedlin and J. Orcutt (Birkhäuser,Basel, Switzerland), pp. 475–512.

Dushaw, B. D., and Menemenlis, D. (**2014**). "Antipodal acoustic thermometry: 1960, 2004," Deep Sea Res. Part I **86**, 1–20.

Dushaw, B. D., Worcester, P. F., Munk, W. H., Spindel, R. C., Mercer, J. A., Howe, B. M., Metzger, K., Jr., Birdsall, T. G., Andrew, R. K., Dzieciuch, M. A., Cornuelle, B. D., and Menemenlis, D. (**2009**). "A decade of acoustic thermometry in the North Pacific Ocean," J. Geophys. Res. Oceans **114**(C7), C7, https://doi.org/10.1029/2008JC005124.

Evers, L., Wapenaar, K., Heaney, K., and Snellen, M. (**2017**). "Deep ocean sound speed characteristics passively derived from the ambient acoustic noise field," Geophys. J. Int. **210**(1), 27–33.
Forget, G., Campin, J.-M., Heimbach, P., Hill, C. N., Ponte, R. M., and Wunsch, C. (**2015**). "ECCO version 4: An integrated framework for non-linear inverse modeling and global ocean state estimation," Geosci. Model Dev. **8**(10), 3071–3104.
Fox, C. G., Matsumoto, H., and Lau, T.-K. A. (**2001**). "Monitoring Pacific Ocean seismicity from an autonomous hydrophone array," J. Geophys. Res. Solid Earth **106**(B3), 4183–4206, https://doi.org/10.1029/2000JB900404.
GEBCO (**2023**). "GEBCO 2023 Grid," https://www.gebco.net/data-products/gridded-bathymetry-data/gebco2023-grid.
Gemba, K. L., Durofchalk, N. C., Dall'Osto, D. R., Andrew, R. K., Leary, P., Howe, B. M., and Smith, K. B. (**2023**). "Basin scale coherence of Kauai-Beacon m-sequence transmissions received at Wake Island and Monterey, CA," JASA Express Lett. **3**(8), 080801.
Godin, O. A. (**2021**). "Contributions of gravity waves in the ocean to T-phase excitation by earthquakes," J. Acoust. Soc. Am. **150**(5), 3999–4017.
Graeber, F. M., and Piserchia, P.-F. (**2004**). "Zones of T-wave excitation in the NE Indian ocean mapped using variations in backazimuth over time obtained from multi-channel correlation of IMS hydrophone triplet data," Geophys. J. Int. **158**(1), 239–256.
Igarashi, T. (**2020**). "Catalog of small repeating earthquakes for the Japanese Islands," Earth. Planets Space **72**, 73.
Intergovernmental Panel on Climate Change (**2021**). "Working Group I of the IPCC assesses the physical science of climate change," https://www.ipcc.ch/report/ar6/wg1/about/working-group/.
Johnson, R. H., Northrop, J., and Eppley, R. (**1963**). "Sources of Pacific T phases," J. Geophys. Res. **68**(14), 4251–4260, https://doi.org/10.1029/JZ068i014p04251.
Lecoulant, J., Oliveira, T. C. A., and Lin, Y.-T. (**2021**). "Three-dimensional modeling of T-wave generation and propagation from a South Mid-Atlantic Ridge earthquake," J. Acoust. Soc. Am. **150**(5), 3807–3824.
Munk, W. H. (**1980**). "Horizontal deflection of acoustic paths by mesoscale eddies," J. Phys. Oceanogr. **10**(4), 596–604.
Munk, W. H., Worcester, P., and Wunsch, C. (**1995**). *Ocean Acoustic Tomography* (Cambridge University Press, Cambridge, UK).
Munk, W., and Wunsch, C. (**1979**). "Ocean acoustic tomography: A scheme for large scale monitoring," Deep Sea Res. Part A **26**(2), 123–161.
Nichols, S. M., and Bradley, D. L. (**2017**). "*In situ* shape estimation of triangular moored hydrophone arrays using ambient signals," IEEE J. Oceanic Eng. **42**(4), 923–935.
Okal, E. A. (**2008**). "The generation of T waves by earthquakes," in *Advances in Geophysics*, edited by R. Dmowska (Academic Press, San Diego, CA), Vol. 49, pp. 1–65.
Oliveira, T. C. A., Metz, D., Lin, Y.-T., Saragiotis, C., and Begnaud, M. L. (**2024**). "Conversion from seismic to underwater sound waves along the Louisville Seamount Chain," J. Acoust. Soc. Am. **155**(5), 3371–3379.
Park, M., Odom, R. I., and Soukup, D. J. (**2001**). "Modal scattering: A key to understanding oceanic T-waves," Geophys. Res. Lett. **28**(17), 3401–3404, https://doi.org/10.1029/2001GL013472.
Peng, S., and Callies, J. (**2025**). "Estimating temperature variability and trends from a combination of seismic and *in situ* data," Proc. R. Soc. A **481**(2313), 20240494.
Peng, S., Callies, J., Nagura, M., and Mcphaden, M. J. (**2025**). "Yanai waves in the deep East Indian Ocean observed with seismic ocean tomography," J. Phys. Oceanogr. **55**, 471–488.
Peng, S., Callies, J., Wu, W., and Zhan, Z. (**2024**). "Seismic ocean thermometry of the Kuroshio Extension region," J. Geophys. Res. Oceans **129**(2), e2023JC020636, https://doi.org/10.1029/2023JC020636.
Ragland, J., Abadi, S., and Sabra, K. (**2024**). "Using ocean ambient sound to measure local integrated deep ocean temperature," Geophys. Res. Lett. **51**(12), e2024GL108943, https://doi.org/10.1029/2024GL108943.
Shen, Z., Wu, W., and Callies, J. (**2024**). "Genesis and propagation of low-frequency abyssal T-waves," J. Geophys. Res. Oceans **129**(10), e2024JC021518, https://doi.org/10.1029/2024JC021518.
Simon, J. D., Simons, F. J., Irving, J. C. E., Wu, W., Obayashi, M., Yu, Y., Chen, Y. J., Sugioka, H., and Hello, Y. M. (**2025**). "Hydroacoustic observations of the 15 January 2022 Hunga Tonga-Hunga Ha'apai eruption: The role of bathymetry along the path," *ESS Open Archive*.
Smets, P. S. M., Weemstra, C., and Evers, L. G. (**2022**). "Hydroacoustic travel time variations as a proxy for passive deep-ocean thermometry—a cookbook," J. Geophys. Res. Oceans **127**(5), e2022JC018451, https://doi.org/10.1029/2022JC018451.
Talandier, J., and Okal, E. A. (**1998**). "On the mechanism of conversion of seismic waves to and from T waves in the vicinity of island shores," Bull. Seismol. Soc. Am. **88**(2), 621–632
Talley, L. D., Feely, R. A., Sloyan, B. M., Wanninkhof, R., Baringer, M. O., Bullister, J. L., Carlson, C. A., Doney, S. C., Fine, R. A., Firing, E., Gruber, N., Hansell, D. A., Ishii, M., Johnson, G. C., Katsumata, K., Key, R. M., Kramp, M., Langdon, C., Macdonald, A. M., Mathis, J. T., McDonagh, E. L., Mecking, S., Millero, F. J., Mordy, C. W., Nakano, T., Sabine, C. L., Smethie, W. M., Swift, J. H., Tanhua, T., Thurnherr, A. T., Warner, M. J., and Zhang, J.-Z. (**2016**). "Changes in ocean heat, carbon content, and ventilation: A review of the first decade of GO-SHIP global repeat hydrography," Annu. Rev. Mar. Sci. **8**, 185–215.
Tan, T. W., and Godin, O. A. (**2021**). "Passive acoustic characterization of sub-seasonal sound speed variations in a coastal ocean," J. Acoust. Soc. Am. **150**(4), 2717–2737.
The ATOC Consortium (**1998**). "Ocean climate change: Comparison of acoustic tomography, satellite altimetry, and modeling," Science **281**(5381), 1327–1332.
Tolstoy, M., and Bohnenstiehl, D. R. (**2005**). "Hydroacoustic constraints on the rupture duration, length, and speed of the great Sumatra-Andaman earthquake," Seismol. Res. Lett. **76**(4), 419–425.
Wong A. P. S., Wijffels S. E., Riser S. C. *et al.* (**2020**). "Argo data 1999–2019: Two million temperature-salinity profiles and subsurface velocity observations from a global array of profiling floats," Front. Mar. Sci. **700**, 7.
Woolfe, K. F., Lani, S., Sabra, K. G., and Kuperman, W. A. (**2015**). "Monitoring deep-ocean temperatures using acoustic ambient noise," Geophys. Res. Lett. **42**(8), 2878–2884, https://doi.org/10.1002/2015GL063438.
Wu, W., Shen, Z., Peng, S., Zhan, Z., and Callies, J. (**2023**). "Seismic ocean thermometry using CTBTO hydrophones," J. Geophys. Res. Solid Earth **128**(9), e2023JB026687, https://doi.org/10.1029/2023JB026687.
Wu, W., Zhan, Z., Peng, S., Ni, S., and Callies, J. (**2020**). "Seismic ocean thermometry," Science **369**(6510), 1510–1515.